Mühendis ve Makina
cilt 63, sayı 709, s. 672-688, 2022
Araştırma Makalesi

Engineer and Machinery
vol. 63, no. 709, p. 672-688, 2022
Research Article

DOI : 10.46399/muhendismakina.1139121

Eccentricity in a Horizontal Latent Thermal Energy Storage Unit: Effects of Inner Tube Geometry

Özgür Bayer[1]

ABSTRACT

The intermittency of solar energy has resulted in a urge to implement a buffer for providing constant and reliable energy in different sectors. Latent thermal energy storage solutions that use phase change materials have been the main focus of researchers due to their size, cost and near-constant operating temperatures. One of the main ways of performance improvement in concentric LTES units is changing the location of inner tube to introduce eccentricity and decrease the response and charging time of the unit. In this study, the eccentricity is implemented for different inner tube geometries, circle, square and triangle. The time dependent melting behavior of all the cases are presented by investigating the velocity, temperature and liquid fraction contours. The melting time is improved for all the cases with the triangle eccentric design having the lowest melting time. The charge time in the triangular case is decreased nearly 50% while the decrease is less significant for the circle and square designs. The natural convection improvement due to employment of eccentricity is the reason for the enhancements.

Keywords: PCM, natural convection, melting, thermal battery

Bir Yatay Gizli Isıl Enerji Depolama Biriminde Eksantriklik: İç Boru Geometrisinin Etkileri

ÖZ

Güneş enerjisinin kesintili karakteristiği, farklı sektörlerde süreklilik arz eden ve güvenilir enerji sağlamak amaçlı uygulamaların geliştirilmesini teşvik etmektedir. Faz değiştiren malzemelerin kullanıldığı gizli ısıl enerji depolama çözümleri, boyutları, maliyetleri ve sabite yakın çalışma sıcaklıkları nedeniyle araştırmacıların ana odak noktası olmuştur. Eş merkezli LTES ünitelerinde performans iyileştirmesi için temel yöntemlerden bir tanesi, eksantrikliği sağlamak ve ünitenin tepki ve şarj süresini azaltmak için iç borunun konumunu değiştirmektir. Bu çalışmada, daire, kare ve üçgen şeklindeki farklı iç boru geometrileri için eksantriklik uygulaması gerçekleştirilmiştir. Tüm durumlar için zamana bağlı erime davranışı hız, sıcaklık ve sıvı fraksiyonu konturları incelenerek sunulmuştur. Tüm durumlar için en düşük erime süresine sahip üçgen eksantrik tasarım ile erime süresinin en optimum şekilde iyileştirildiği gözlemlenmiştir. Üçgen tasarımda şarj süresi yaklaşık %50 azalırken, daire ve kare tasarımlarda bu azalma daha az belirgindir. Eksantrikliğin kullanılmasından kaynaklanan doğal konveksiyon performansındaki artış, erime süresindeki iyileşmelerin temel nedenidir.

Anahtar Kelimeler: FDM, doğal taşınım, erime, termal pil

Geliş/Received : 02.07.2022
Kabul/Accepted : 08.09.2022

[1] Middle East Technical University, Department of Mechanical Engineering, Çankaya, Ankara, Turkey
bayer@metu.edu.tr, ORCID:0000-0003-0508-2263

1. INTRODUCTION

Intermittency is one of the primary problems with solar energy and its role in mitigating the consumption of fossil fuels and global warming. Solar energy is stored in the form of heat, which renders the application of thermal energy storage (TES) systems a viable solution for achieving a continuous energy supply during days and nights [1]. TES units are generally categorized into sensible, latent, and chemical. The sensible TES systems are mostly large due to their small specific heat capacity, and chemical TES units are still being developed and are faced with various challenges such as stability problems. On the other hand, latent TES (LTES) systems, due to their sizeable latent heat during the melting/solidification process, introduced a type of TES that is small scale and large in energy capacity [2].

The main problem with LTES is the low thermal conductivity of phase change material (PCM) which results in low rates of charging and discharging. Researchers have developed various methods to combat this deficiency. Using extended surfaces such as fins in the design of a TES tank [3-5], nanomaterials induced in the PCM to increase its thermal conductivity value [6-8], porous media [9-11] and encapsulation [12-14] have proven to be effective ways to increase the performance of LTES. However, since the simplest and most common type of TES tank is the shell-and-tube type, many researchers have focused on modifying the heat exchanger to achieve better charging/discharging rates. The shell-and-tube type tank usually consists of two concentric tubes where a heat transfer fluid flows in the inner tube, and the space between the tubes is filled with PCM. In the charging process, hot fluid is flown in the inner tube which results in melting of the PCM. The melting process is mainly dominated by natural convection both in horizontal and vertical TES tank configurations [15].

One of the recent modifications in the literature is changing the location of the inner tube to modify the effects of natural convection in the horizontal configuration. Yazıcı et al. [16] conducted an experimental study of eccentricity on the charging process of a horizontal shell-and-tube storage unit. Three eccentricity values were examined, with the maximum value having the best performance. They concluded that by lowering the tube, the natural convection is enhanced. Melting time decreases of up to 67% were reported compared to concentric configuration. Pahamli et al. [17] performed a series of numerical studies to observe the effects of operating parameters (temperature and mass flow rate) alongside eccentricity in a single-pass horizontal LTES. Modes of heat transfer (conduction at the beginning and ending and natural convection during the charging process) were analyzed. They established that by increasing the eccentricity, the area for natural convection to take place increases, resulting in a shorter melting time (up to 64%). Cao et al. [18] experimentally and numerically investigated the melting performance in a horizontal LTES with changing the boundary conditions and eccentricity to improve the melting time. A decrease of 57% in charging time

was reported. By defining an average convective heat transfer coefficient, particular attention was paid to the progression of natural convection. It was concluded that the eccentric case has a larger average convective heat transfer coefficient value, thus a better charging performance. Kumar and Verma [19] performed experimental and numerical investigations to study the behavior of using longitudinal fins alongside tube eccentricity in a lauric acid LTES unit. The goal was to improve the effects of natural convection by using the minimum length for the fins. The maximum eccentricity experienced a 21% enhancement in melting time compared to the finned case in the concentric configuration. Zhang et al. [20], using thermal and exergetic analyses, concluded that the eccentricity is a critical factor when designing an LTES tank is considered. By keeping the mass flow constant, Safari et al. [21] compared six types of longitudinal fins (with bifurcation) and combined these fin designs with eccentric tube configurations. The eccentric design resulted in a lower melting time, up to 54%. On the other hand, although the bifurcations increased the total heat transfer rate, natural convection was hindered. Khan et al. [22] used the enthalpy porosity method in a two-dimensional numerical model to investigate the effects of eccentricity, fin design, and addition of nanoparticles for PCM thermal conductivity enhancement in a horizontal shell-and-tube type LTES. An optimized eccentricity value was established for which the melting time was reduced to 34.14% and the rate of thermal energy storage was increased by 30.7% compared to zero eccentricity. Zhou et al. [23] suggested a parameter (eccentric space ratio) with which the performance of an eccentric LTES is determined. They performed a series of 3D numerical simulations to establish the effects of different space ratios. More recently, Patel et al. [24] examined the eccentricity of the inner tube alongside the addition of fins and concluded that their combination results in the fastest melting time though eccentricity is not effective when solidification is considered, which is mostly dominated by conduction.

Considering the presented literature review, most studies investigate the magnitude of eccentricity and inclusion of fins in the charging process without studying the effects of the eccentric tube geometry. In the present study, at a constant eccentricity value, three different tube geometries, circular, square, and triangular, with and without eccentricities, are considered for investigation. 2D phase change numerical models are based on the enthalpy porosity method, while the natural convection is handled using Boussinesq approximation.

2. METHODOLOGY

2.1 Numerical Domains

A base geometry originating from the benchmark study of Darzi et al. [25] is first considered to examine the effects of different tube geometries in concentric and eccentric configurations. The base circular geometry consists of concentric circles with

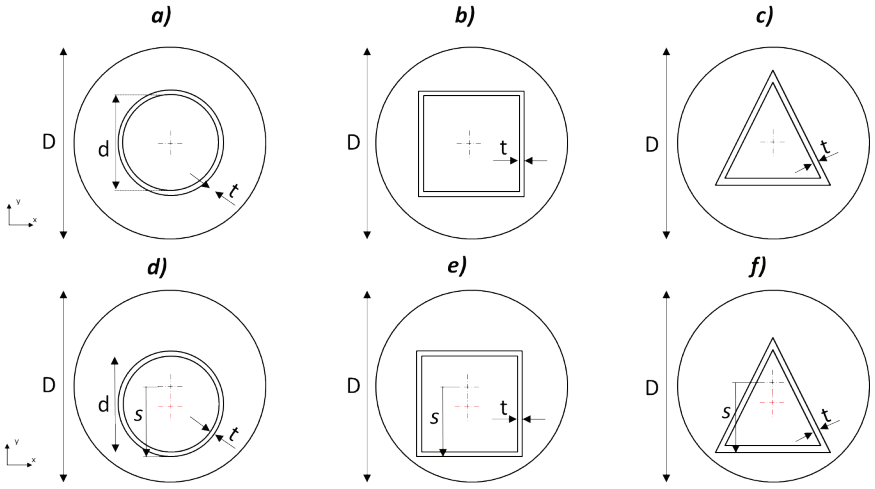

Figure 1. Numerical Domains and The Relevant Dimensions For Concentric a) Circle-Circle (CCC) b) Circle-Square (CCS) and c) Circle-Triangle (CCT) Tube Geometries and Eccentric d) Circle-Circle (ECC) e) Circle-Square (ECS) and f) Circle-Triangle (ECT) Geometries

Table 1. Properties of N-eicosane [25]

Melting range (°C)	Density (kg/m^3)	Kinematic viscosity (m^2/s)	Specific heat capacity (J/kgK)	Thermal conductivity (W/mK)	Latent heat of fusion (kJ/kg)	Thermal expansion coefficient (1/K)
35-37	770	5×10^{-6}	2460	0.1505	247.6	0.0009

the inner cylinder with an inner diameter of d = 20mm and thickness of t = 1.5mm and an outer circle with a diameter of D = 40mm. For the square and equilateral geometry cases, the PCM area and thickness of the inner tube are kept constant. The center to outer shell value of s = 12mm is given to all the cases which represents the eccentricity. This value is chosen such that the triangular case contains a minimum distance to the outer shell. The studied cases with the relevant dimensions are depicted in Fig. 1.

The space between the inner and outer tubes is filled with N-eicosane [25] PCM, the properties of which are given in Table 1. The shell of the inner tube is made of copper (k = 400 W/mK).

2.2 Governing Equations, Initial and Boundary Conditions

The numerical model of the proposed configurations is based on the following assumptions:

- The flow is unsteady, laminar, two dimensional, and incompressible
- Viscous dissipation is negligible
- The properties are constant and temperature independent

The continuity and momentum in x and y-directions are as given in Eqns. 1 to 3 in the Cartesian coordinate system, respectively.

$$\frac{\partial u}{\partial x}+\frac{\partial v}{\partial y}=0 \tag{1}$$

$$\rho_f\left(\frac{\partial u}{\partial t}+u\frac{\partial u}{\partial x}+v\frac{\partial u}{\partial y}\right)=\mu\left(\frac{\partial^2 u}{\partial x^2}+\frac{\partial^2 u}{\partial y^2}\right)-\frac{\partial p}{\partial x}+S_x \tag{2}$$

$$\rho_f\left(\frac{\partial v}{\partial t}+u\frac{\partial v}{\partial x}+v\frac{\partial v}{\partial y}\right)=\mu\left(\frac{\partial^2 v}{\partial x^2}+\frac{\partial^2 v}{\partial y^2}\right)-\frac{\partial p}{\partial y}+S_y+\rho_f g\beta\left(T-T_{ref}\right) \tag{3}$$

where ρ_f, u, v, μ, p and β are fluid density, velocity in the x-direction, velocity in the y-direction, dynamic viscosity, pressure, and coefficient of thermal expansion. The $\rho_f g\beta\,(T\text{-}T_{ref})$ term refers to the Boussinesq approximation and S_x and S_y are the source terms used to account for melting/solidification modeling based on enthalpy porosity method [26] defined in Eqns. 4 and 5.

$$S_x=C_{mush}\frac{\left(1-\gamma\right)^2}{\gamma^3+\varepsilon}u \tag{4}$$

$$S_y=C_{mush}\frac{\left(1-\gamma\right)^2}{\gamma^3+\varepsilon}v \tag{5}$$

where γ is the liquid fraction varying between 0 and 1 based on PCM temperature:

$$\gamma=\begin{cases}0 & T<T_{solid}\\ \dfrac{T-T_{solid}}{T_{liquid}-T_{solid}} & T_{solid}<T<T_{liquid}\\ 1 & T>T_{liquid}\end{cases} \tag{6}$$

ε is a small value (0.001) to avoid division by zero and C_{mush} is a large value (here taken as 10^5) which controls the amount of velocity damping in the mushy zone when the melting happens.

The conservation of energy is given as:

$$\rho_f \left(\frac{\partial h}{\partial t} + \frac{\partial}{\partial x}(uh) + \frac{\partial}{\partial y}(vh) \right) = \frac{\partial}{\partial x}\left(k_f \frac{\partial T}{\partial x} \right) + \frac{\partial}{\partial y}\left(k_f \frac{\partial T}{y} \right) \tag{7}$$

in which T is the temperature and k_f is the fluid thermal conductivity. The total specific enthalpy, h, is comprised of sensible and latent components:

$$h = h_s \, \Delta \, h_L \tag{8}$$

where h_s is the specific sensible enthalpy:

$$h_s = h_{s0} + \int_{T_0}^{T} C_p dT \tag{9}$$

Δh_L which indicates the change of specific enthalpy due to phase change, is defined based on latent heat of fusion as:

$$\Delta h_L = \gamma_L \tag{10}$$

where L is the latent heat of fusion.

For the solid thickness between the inner and outer tube, the transient conduction equation is applied as:

$$\frac{\partial^2 T}{\partial x^2} + \frac{\partial^2 T}{\partial y^2} = \frac{1}{\alpha} \frac{\partial T}{\partial t} \tag{11}$$

where α is the thermal diffusivity.

The outer shell of the LTES is insulated while a constant temperature of 56°C is applied to the inner tube's interior wall, and initially, all the domains are at 35°C.

The pressure and velocity are coupled using the SIMPLE algorithm. The second-order upwind scheme was used to discretize the momentum and energy equations, while the PRESTO scheme calculated the pressure term. ANSYS FLUENT commercial software was employed for solving the sets of equations with the relevant boundary and initial conditions.

2.3 Validation and Mesh Independency

To validate the current numerical model, the CCC case is created based on the study of Darzi et al., and the time-dependent behavior of the area-averaged PCM liquid fraction in the melting process is compared in Fig.2. A maximum error of 4.43% is attained for the current numerical code compared to the study by Darzi et al.

To study the effects of mesh on the charging process, the ECC case is considered with

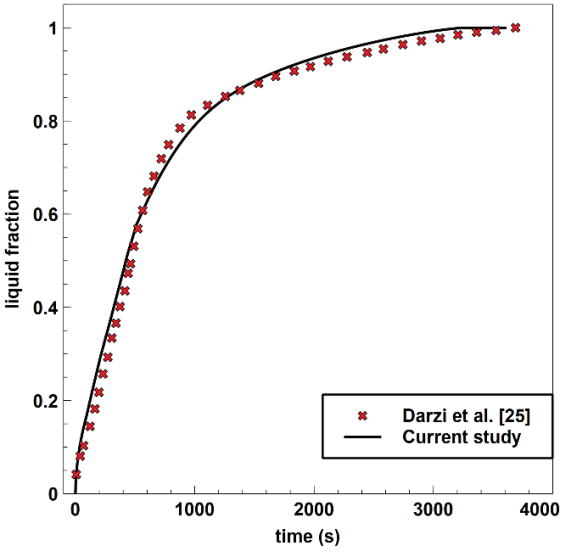

Figure 2. Comparison of Liquid Fraction Between The Current Study and the Study Performed by Darzi et al. for the Validation

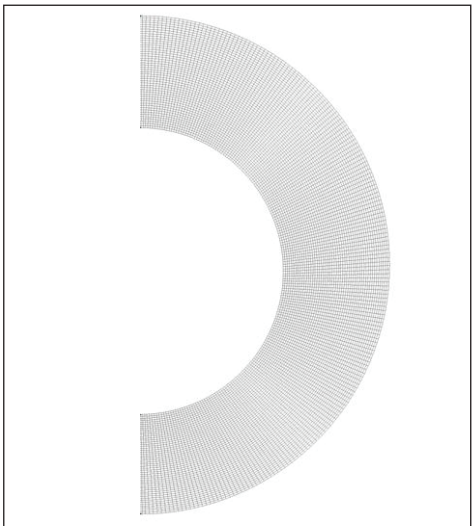

Figure 3. The Chosen Mesh Configuration as a Result of Mesh Independency Study

three different mesh configurations: 4523, 9810, and 18900 elements. For comparison, the total charging time was accounted for the mentioned meshes, and the mesh with 9810 differed by only 0.11%. Therefore, the configuration with 9810 element

numbers was chosen for further simulations. The chosen mesh is presented in Fig. 3. It is worth noting that a similar meshing was used for the square and triangle cases.

3. RESULTS

Fig. 4a to 4c compares the effect of eccentricity on the time-dependent liquid fraction of circle (CCC and ECC), square (CCS and ECS), and triangle (CCT and ECT) cases presented in Fig. 1. d, e and f. It is evident that the eccentricity shortens the melting time no matter the geometry though this improvement is less significant in the circle configuration (ECT) and most prominent in the triangular case (ECT). The behavior of the liquid fraction graphs indicates that natural convention is the main mode of heat transfer in the triangular case. More than 95% of the melting in the ECT configuration is done by natural convection, while this value is less than 80% for the ECC. Fig. 4a suggests that in the circular case, even by addition of eccentricity, a small non-melted

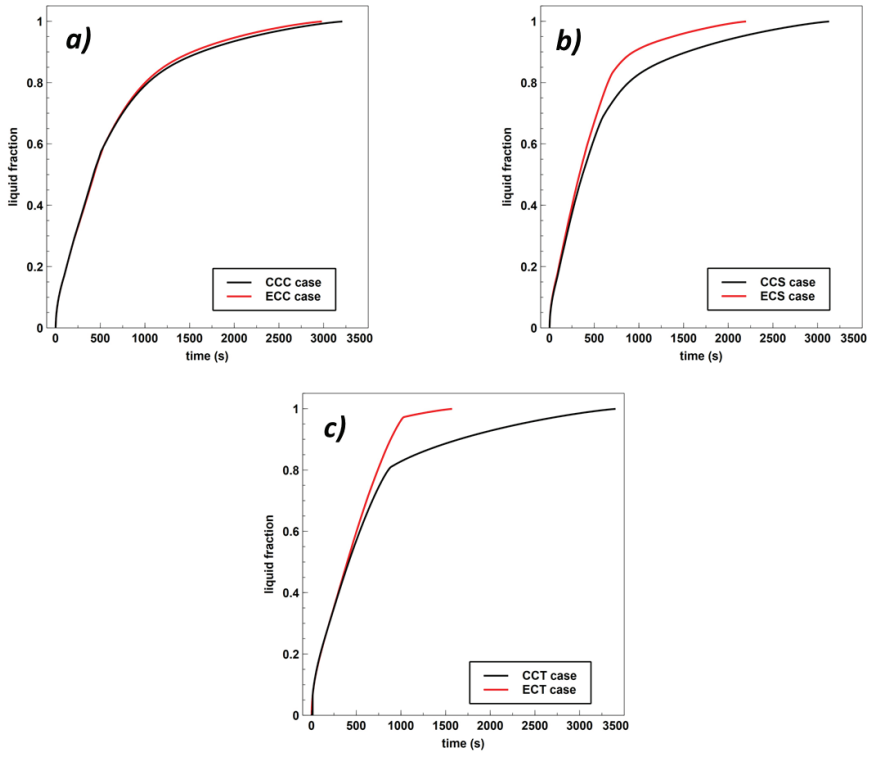

Figure 4. Time-Dependent Behavior of Liquid Fraction for a) CCC and ECC b) CCS and ECS and c) CCT and ECT Cases

PCM exists at the bottom of the container. This non-melted PCM is less in the square case and the smallest in the triangle design.

In addition, a very sharp change in the characteristics of the CCT and ECT cases is observed. The reason is that due to the geometry of the triangle, once the PCM melts in the vicinity of two sides, the bottom part remains nearly intact from the convective flows, and the heat transfer suddenly changes to conduction at the bottom of the container, where some solid PCM still exists. The conduction dominancy of the isolated region arises from the fact that the heated surfaces is at the top of the non-melted PCM which does not trigger the natural convection.

To better investigate and understand the underlying effects of eccentricity, temperature, velocity, and liquid fraction contours of the CCC and ECC, CCS and ECS and CCT and ECT configurations are depicted in Fig. 5 to 10 in times of 10mins to 30mins after melting process starts. It is important to note that the temperature and velocity are depicted in one figure (left side) due to symmetry.

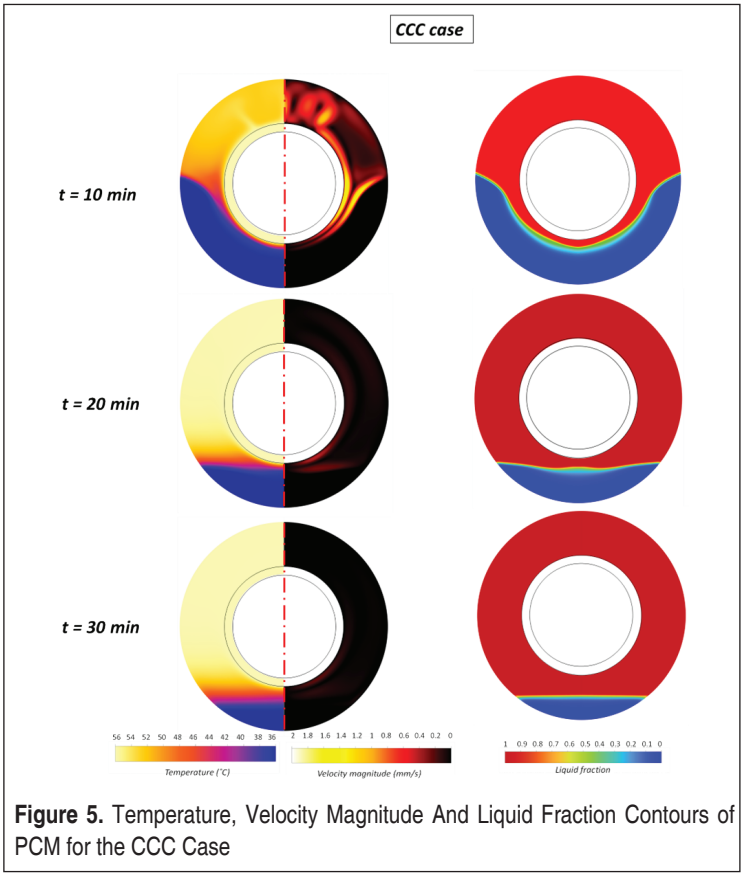

Figure 5. Temperature, Velocity Magnitude And Liquid Fraction Contours of PCM for the CCC Case

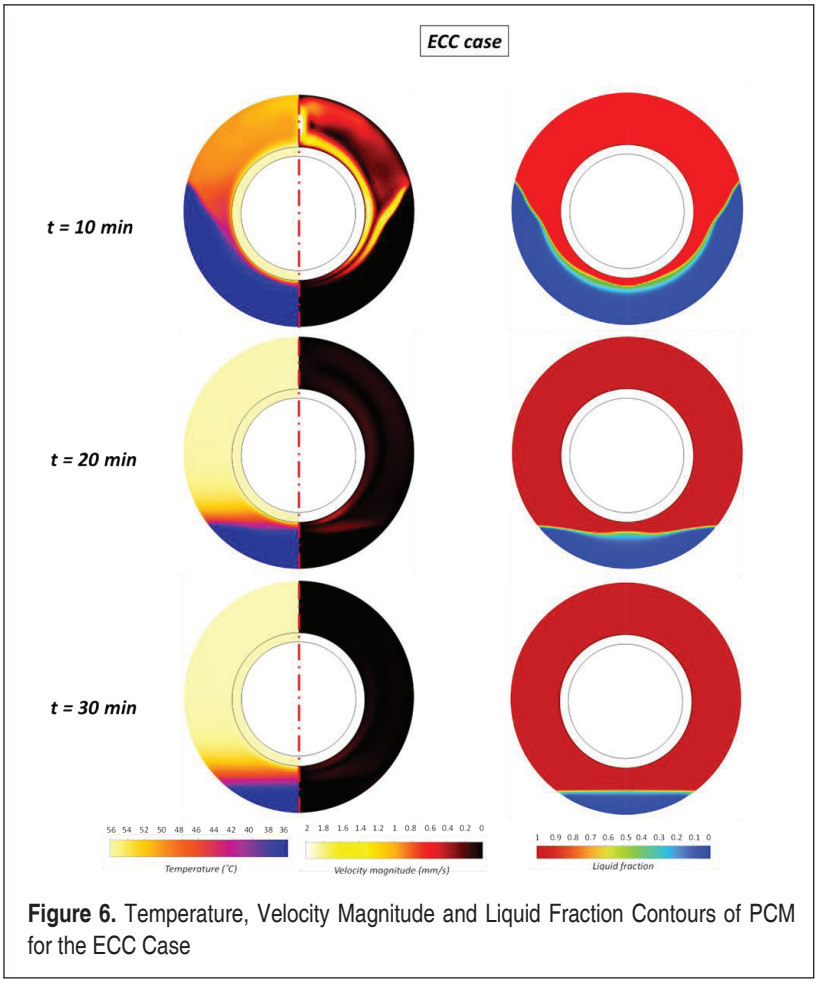

Figure 6. Temperature, Velocity Magnitude and Liquid Fraction Contours of PCM for the ECC Case

When all the geometries are compared, it is observed that the eccentricity results in better melting and smaller amount of solid PCM is left at the bottom of the container when eccentricity exists. The velocities due to natural convection get more significant for the circle design as the eccentricity is introduced (comparing Fig. 5 to Fig. 6 at time = 10min). The same behavior is observed for the square and triangular designs. By comparing CCS and ECS cases it is established that, for the square case, a large velocity in the melted region results in better mixing and thus faster melting.

With the introduction of the eccentricity, the natural convection is improved in the first 10 minutes, which indicates that even a small amount of eccentricity can affect the melting response. Even though the melting is improved, there still exists a small amount of solid PCM at the bottom of the container suggesting a further increase of

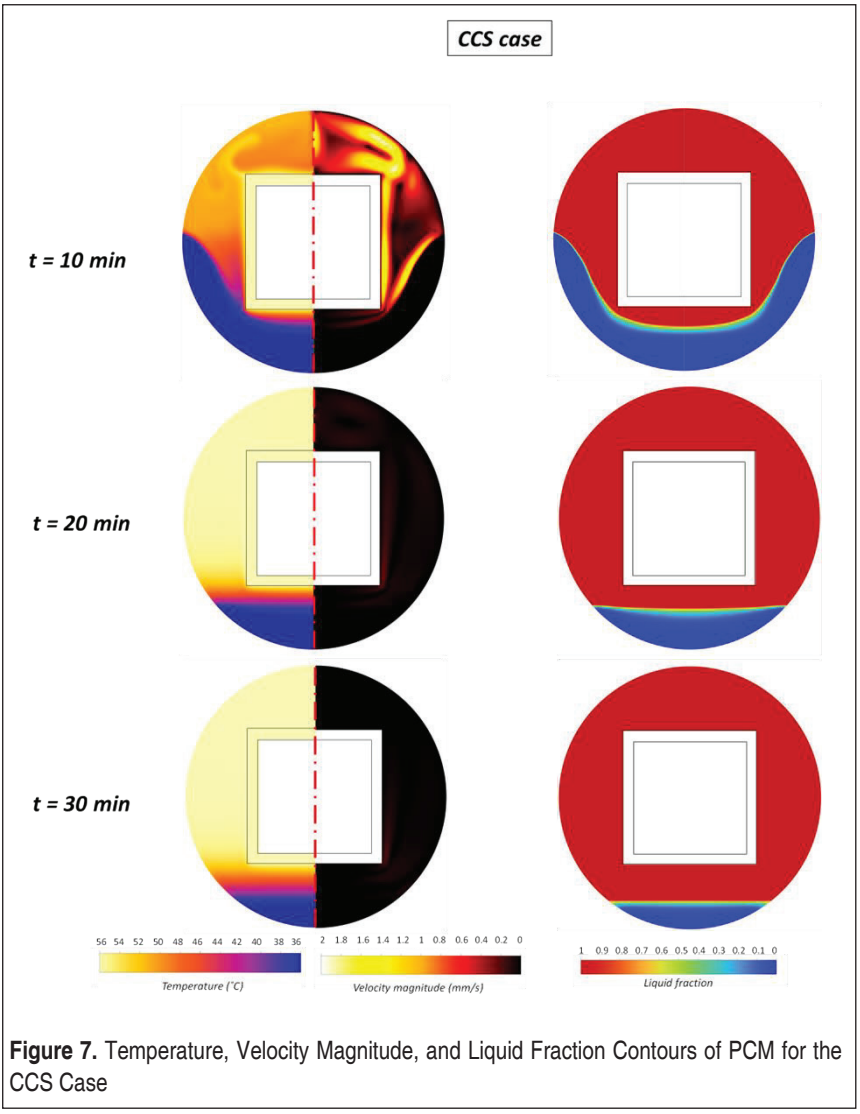

Figure 7. Temperature, Velocity Magnitude, and Liquid Fraction Contours of PCM for the CCS Case

eccentricity would be beneficial for decreasing the melting time.

The ECT case is the only case that is fully melted 30mins after the melting starts, which indicates that the natural convection is maximized on the two sides of the triangle. The natural convection on the sides of the triangle act similar to the classical natural convection flows in tilted flat plates, which has been shown to have a higher convective heat transfer coefficient when compared to the vertical configuration [27]. In this configuration, due to eccentricity, the two bottom edges of the triangle nearly

trap a slight amount of PCM at the bottom of the outer shell, resulting in a conduction-dominant melting at that location. The sharp change of behavior in the liquid fraction time-dependent profile of the eccentric triangle case (Fig. 4c) can be explained by Fig.10. The top region of the PCM is melted quickly, which is dominated by convection, which results in a sharp increase of liquid fraction and, therefore a fast response of PCM. Then, the small solid PCM region melts, which is conduction dominant. Since the thermal conductivity of PCMs is low, the melting response in the bottom trapped region is slower, as depicted in Fig.4c.

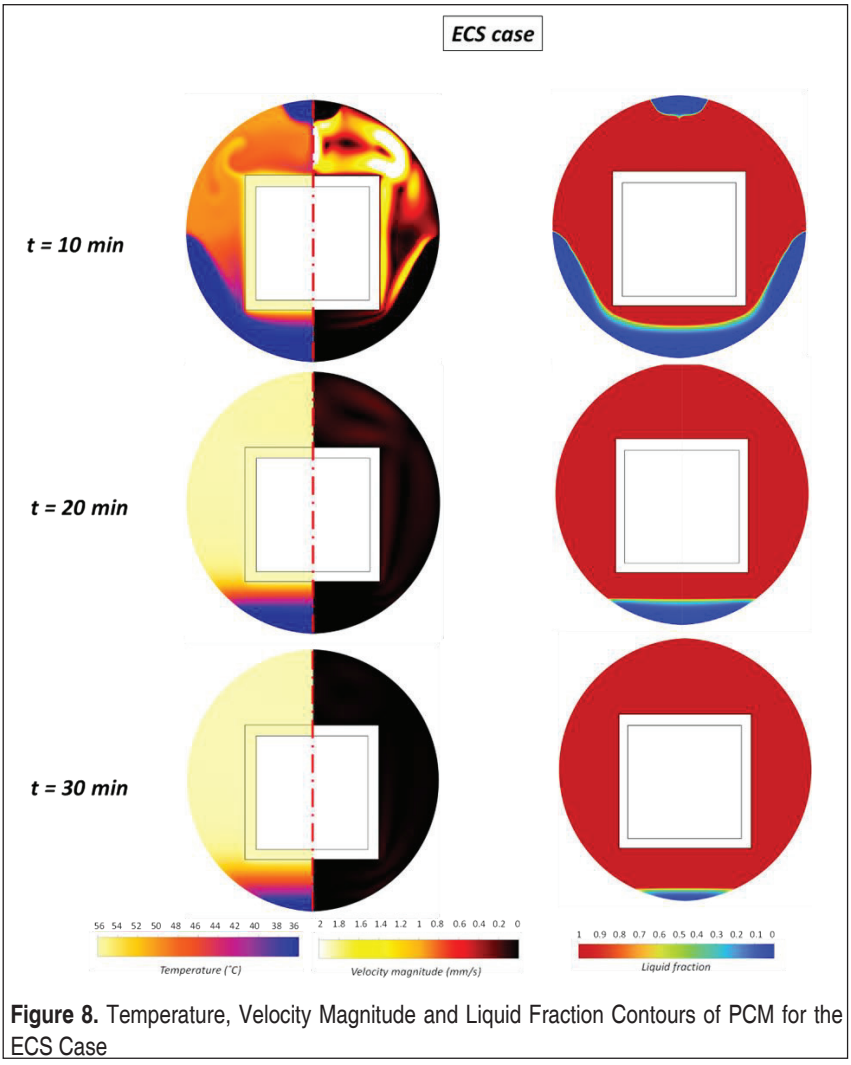

Figure 8. Temperature, Velocity Magnitude and Liquid Fraction Contours of PCM for the ECS Case

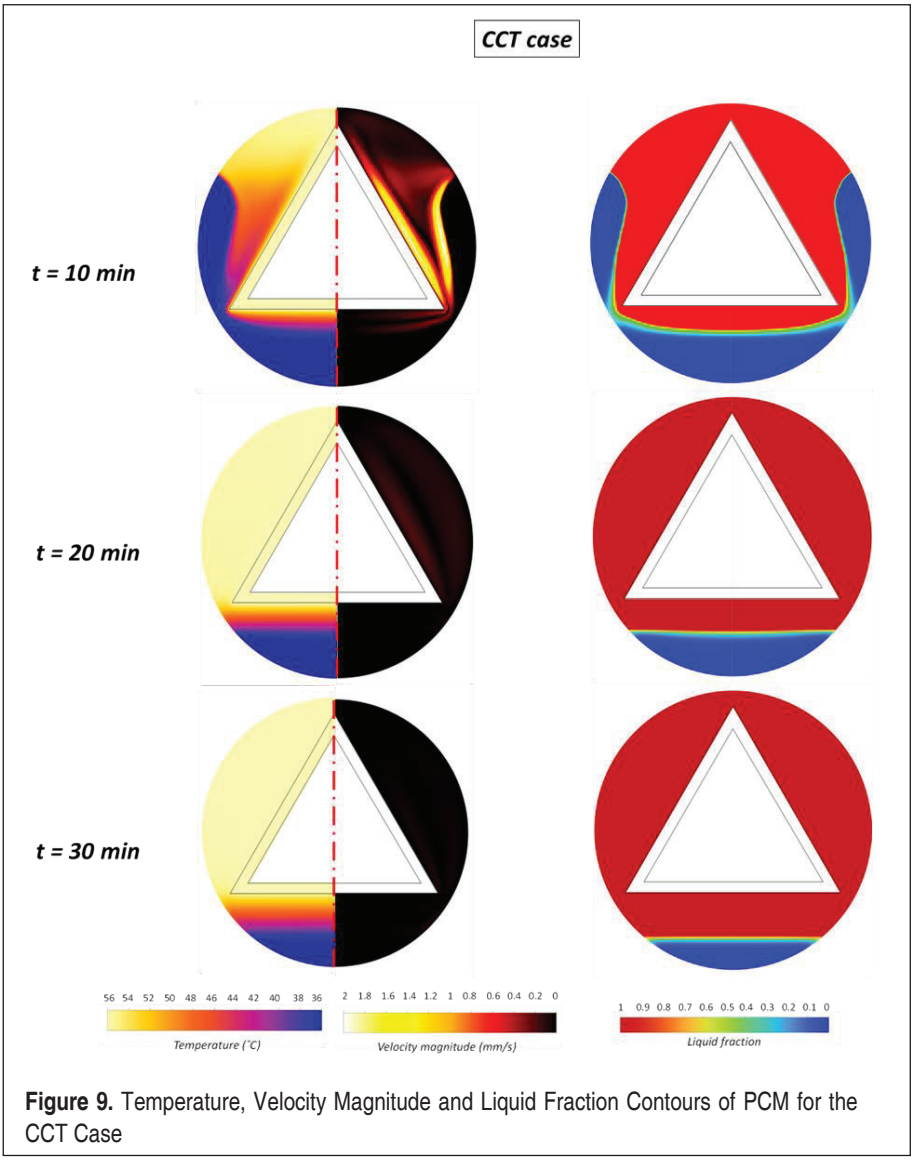

Figure 9. Temperature, Velocity Magnitude and Liquid Fraction Contours of PCM for the CCT Case

Table 2 compares the full melting time of all the cases. The CCT case has the longest melting time, while the ECT case has the shortest charging time. Since the CCT case extends to the upper region of the container, a smaller area is left for the natural convection to act. However, when the eccentricity is added, this deficiency is minimized, and the melting time is shortened significantly. With the eccentricity, the triangular case has the shortest heated surface distance to the bottom of the container, resulting

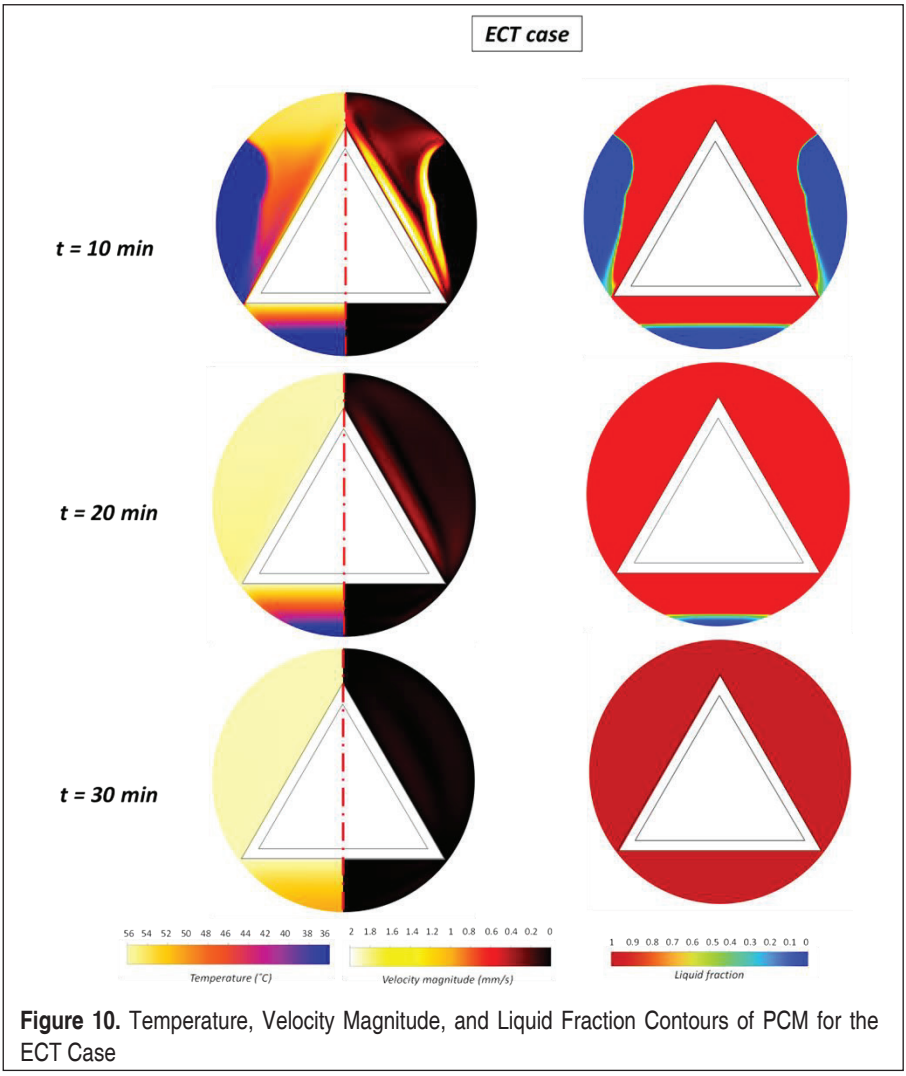

Figure 10. Temperature, Velocity Magnitude, and Liquid Fraction Contours of PCM for the ECT Case

Table 2. Comparison of Melting Time For All the Casee

case	melting time (min)
CCC	53.3
ECC	49.5
CCS	52
ECS	36.5
CCT	56.5
ECT	26

in a smaller thermal resistance between the bottom side of the triangle and the solid PCM.

4. CONCLUSION AND SUGGESTIONS

Three different geometries with and without eccentricity were numerically investigated for an LTES unit. The numerical code based on FVM was validated using the data from the literature. The time dependent behavior of liquid fractions for each case was examined while the contours of velocity, temperature, and liquid fraction were presented for different time intervals. The main findings of the current work are listed below:

1. Even a small amount of eccentricity results in a enhancement no matter the shape of the inner shell.
2. With the addition of eccentricity, the natural convection is enhanced in all the cases.
3. When no eccentricity exists, the square design has the shortest melting time.
4. The eccentricity affects the triangular case the most, with an almost 54% decrease in melting time.
5. In the ECT, the heated surface at the bottom of the inner shell nearly creates a closed cavity, resulting in a sharp change of behavior from natural convection to conduction.
6. The triangular design experiences the shortest melting time with eccentricity even though it has the longest melting time when no eccentricity exists.

Therefore, it can be concluded that the eccentricity is important in the circular tube design (which has been extensively studied in the literature) and in various geometries. The triangular case is of great interest since it had the most prominent improvement. As for future work, optimization processes can be employed for the triangular case to study the orientation and dimensions of the triangular inner shell.

REFERENCES

1. **Alva, G., Liu, L., Huang, X., & Fang, G.** (2017). Thermal energy storage materials and systems for solar energy applications. Renewable and Sustainable Energy Reviews, 68, 693-706.
2. **Nkwetta, D. N., & Haghighat, F.** (2014). Thermal energy storage with phase change material—A state-of-the art review. Sustainable cities and society, 10, 87-100.
3. **Kamkari, B., & Shokouhmand, H.** (2014). Experimental investigation of phase change material melting in rectangular enclosures with horizontal partial fins. International Journal of Heat and Mass Transfer, 78, 839-851.
4. **Desai, A. N., Gunjal, A., & Singh, V. K.** (2020). Numerical investigations of fin efficacy

for phase change material (PCM) based thermal control module. International Journal of Heat and Mass Transfer, 147, 118855.

5. **Fan, L., & Khodadadi, J. M.** (2011). Thermal conductivity enhancement of phase change materials for thermal energy storage: a review. Renewable and sustainable energy reviews, 15(1), 24-46.
6. **Kibria, M. A., Anisur, M. R., Mahfuz, M. H., Saidur, R., & Metselaar, I. H. S. C.** (2015). A review on thermophysical properties of nanoparticle dispersed phase change materials. Energy conversion and management, 95, 69-89.
7. **Wong-Pinto, L. S., Milian, Y., & Ushak, S.** (2020). Progress on use of nanoparticles in salt hydrates as phase change materials. Renewable and Sustainable Energy Reviews, 122, 109727.
8. **Tariq, S. L., Ali, H. M., Akram, M. A., Janjua, M. M., & Ahmadlouydarab, M.** (2020). Nanoparticles enhanced phase change materials (NePCMs)-A recent review. Applied Thermal Engineering, 176, 115305.
9. **Ali, H. M., Janjua, M. M., Sajjad, U., & Yan, W. M.** (2019). A critical review on heat transfer augmentation of phase change materials embedded with porous materials/foams. International Journal of Heat and Mass Transfer, 135, 649-673.
10. **Nomura, T., Okinaka, N., & Akiyama, T.** (2009). Impregnation of porous material with phase change material for thermal energy storage. Materials Chemistry and Physics, 115(2-3), 846-850.
11. **Zhou, D., & Zhao, C. Y.** (2011). Experimental investigations on heat transfer in phase change materials (PCMs) embedded in porous materials. Applied Thermal Engineering, 31(5), 970-977.
12. **Khadiran, T., Hussein, M. Z., Zainal, Z., & Rusli, R.** (2015). Encapsulation techniques for organic phase change materials as thermal energy storage medium: A review. Solar Energy Materials and Solar Cells, 143, 78-98.
13. **Su, W., Darkwa, J., & Kokogiannakis, G.** (2015). Review of solid–liquid phase change materials and their encapsulation technologies. Renewable and Sustainable Energy Reviews, 48, 373-391.
14. **Salunkhe, P. B., & Shembekar, P. S.** (2012). A review on effect of phase change material encapsulation on the thermal performance of a system. Renewable and sustainable energy reviews, 16(8), 5603-5616.
15. **Jouhara, H., Żabnieńska-Góra, A., Khordehgah, N., Ahmad, D., & Lipinski, T.** (2020). Latent thermal energy storage technologies and applications: A review. International Journal of Thermofluids, 5, 100039.
16. **Yazıcı, M. Y., Avcı, M., Aydın, O., & Akgun, M.** (2014). Effect of eccentricity on melting behavior of paraffin in a horizontal tube-in-shell storage unit: An experimental study. Solar Energy, 101, 291-298.

17. **Pahamli, Y., Hosseini, M. J., Ranjbar, A. A., & Bahrampoury, R.** (2016). Analysis of the effect of eccentricity and operational parameters in PCM-filled single-pass shell and tube heat exchangers. Renewable energy, 97, 344-357.

18. **Cao, X., Yuan, Y., Xiang, B., & Haghighat, F.** (2018). Effect of natural convection on melting performance of eccentric horizontal shell and tube latent heat storage unit. Sustainable cities and society, 38, 571-581.

19. **Kumar, R., & Verma, P.** (2020). An experimental and numerical study on effect of longitudinal finned tube eccentric configuration on melting behaviour of lauric acid in a horizontal tube-in-shell storage unit. Journal of Energy Storage, 30, 101396.

20. **Zhang, S., Pu, L., Xu, L., & Ma, Z.** (2021). Thermal and exergetic analysis of shell and eccentric-tube thermal energy storage. Journal of Energy Storage, 38, 102504.

21. **Safari, V., Abolghasemi, H., Darvishvand, L., & Kamkari, B.** (2021). Thermal performance investigation of concentric and eccentric shell and tube heat exchangers with different fin configurations containing phase change material. Journal of Energy Storage, 37, 102458.

22. **Khan, L. A., Khan, M. M., Ahmed, H. F., İrfan, M., Brabazon, D., & Ahad, I. U.** (2021). Dominant roles of eccentricity, fin design, and nanoparticles in performance enhancement of latent thermal energy storage unit. Journal of Energy Storage, 43, 103181.

23. **Zhou, H., Wei, L. Y., Cai, Q. L., Ren, X. Z., Bi, C. W., Zhong, D., & Liu, Y.** (2021). Annulus eccentric analysis of the melting and solidification behavior in a horizontal tube-in-shell storage unit. Applied Thermal Engineering, 190, 116752.

24. **Patel, J. R., Rathod, M. K., & Sheremet, M.** (2022). Heat transfer augmentation of triplex type latent heat thermal energy storage using combined eccentricity and longitudinal fin. Journal of Energy Storage, 50, 104167.

25. **Darzi, A. R., Farhadi, M., & Sedighi, K.** (2012). Numerical study of melting inside concentric and eccentric horizontal annulus. Applied Mathematical Modelling, 36(9), 4080-4086.

26. **Brent, A. D., Voller, V. R., & Reid, K. T. J.** (1988). Enthalpy-porosity technique for modeling convection-diffusion phase change: application to the melting of a pure metal. Numerical Heat Transfer, Part A Applications, 13(3), 297-318.

27. **Bergman, T. L., Bergman, T. L., Incropera, F. P., Dewitt, D. P., & Lavine, A. S.** (2011). Fundamentals of heat and mass transfer. John Wiley & Sons.